Materials Research. 2019; 22(suppl. 1): e20180782
DOI: http://dx.doi.org/10.1590/1980-5373-MR-2018-0782

Effect of Etching Temperature on Surface Properties of Ti6Al4V Alloy for Use in Biomedical Applications

Charles Jourdan Alberti*[a], *Eduardo Saito*[b], *Filipe Estevão de Freitas*[b], *Danieli Aparecida Pereira Reis*[b], *João Paulo Barros Machado*[c], *Adriano Gonçalves dos Reis*[a]

[a]*Instituto de Ciência e Tecnologia, Universidade Estadual Paulista (Unesp), São José dos Campos, SP, Brasil*
[b]*Instituto de Ciência e Tecnologia, Universidade Federal de São Paulo, São José dos Campos, SP, Brasil*
[c]*Laboratório Associado de Sensores e Materiais, Instituto Nacional de Pesquisas Espaciais, São José dos Campos, SP, Brasil*

Received: December 01, 2018; Revised: June 10, 2019; Accepted: October 24, 2019.

The objective of this study is to evaluate the surface physicochemical properties of Ti6Al4V alloy after etching with a piranha's solution at temperatures of 25 °C, 40 °C, and 60 °C for 30 min. Scanning electron microscopy with energy-dispersive X-ray spectroscopy, optical profilometry, X-ray diffraction, and wettability analyses were used to characterize the surface of the samples. In addition, corrosion tests were performed using potentiodynamic polarization and electrochemical impedance spectroscopy. The proposed surface treatment did not alter the wettability and surface chemistry (crystallinity), but the texture, surface roughness, superficial area, and corrosion resistance of the alloy could be changed by varying the etching temperature. Considering that these properties are indirect indicators of the alloy's potential success in the osseointegration of a dental implant, the surface treatment of the Ti6Al4V alloy using a piranha solution while controlling the etching temperature has attractive biomedical applications.

Keywords: *Ti6Al4V, surface modification, chemical etching, corrosion resistance, temperature.*

1. Introduction

Titanium and its alloys are among the most biocompatible metallic materials. They possess outstanding mechanical properties, excellent corrosion resistance, and low density (4.42 g/cm^3), which provide them with very high strength-to-weight ratios[1]. Because a surface is the interface where biomaterials meet and interact with the biological environment, surface properties are the major factors ultimately determining the rejection or acceptance of a biomaterial by the body[2]. Surface treatment of biomaterials provides improved biological responses through changes in the material's surface topography, chemistry, energy, and charge while maintaining the bulk properties of the implant unaltered[3].

The surface texture of implants is a determining factor for osseointegration. Depending on the irregularities present on the material's surface, surface roughness can be categorized into three main groups: macroroughness (100 µm–100 mm), microroughness (100 nm–100 µm), and nanoroughness (<100 nm). Each group has a specific influence on cell response[4]. The microtopography of a surface maximizes the interlocking between mineralized bone and the implant surface[5]. Nanoscale surface profiles play an important role in the adsorption of proteins and adhesion of osteoblastic cells and hence in the osseointegration rate[6]. To achieve enhanced bone implant contact, various methods have been developed to create micro- and nanosurfaces, including blasting, acid etching, anodization, and plasma spraying[7-8]. However, many of these treatments are interconnected, and hence, it is almost impossible to control the surface topography without affecting other characteristics of the material, such as wettability and corrosion resistance; therefore, these characteristics must also be evaluated[9].

The wettability of a surface is vitally important for the adsorption of proteins and cell adhesion, and it is considered to be an important criterion for determining the biocompatibility of an implant material[10]. Surfaces with water contact angles between hydrophilic (<30°) and hydrophobic (>90°) ranges are called moderately wettable[11]. For titanium implant surfaces, the contact angle must be in the range 0° (hydrophilic)–140° (hydrophobic)[8].

A criterion for the suitability of a biomaterial in a physiological environment is its physicochemical reactivity. Once the biomaterial is in vivo implanted, it comes in direct contact with body fluids. Body fluids are corrosive aqueous media containing different ions and molecules, such as proteins, polysaccharides, and enzymes, as well as different cells[12]. Most implanted metallic biomaterials have a tendency to lose electrons in solution. As a result, they show a high tendency to undergo corrosion and leak corrosion products or abrasive particles into biological environments, causing inflammation and osteolysis[13]. Ti6Al4V alloy has a stable surface oxide layer that provides excellent corrosion-resistance properties[7].

Several studies have been conducted on the corrosion of titanium and its alloys used as biomaterials[14]. In particular,

*e-mail: adriano.reis@unesp.br

Healy et al.[15] analyzed the oxide layer on biofluids using X-ray photoelectron spectroscopy and Auger electron spectroscopy and revealed the formation of a strong oxide during the first 100 hours of immersion at a growth rate of 0.02 nm/day.

Electrochemical impedance spectroscopy (EIS) combined with other techniques has been widely applied to understand the corrosion resistance of metals, in particular, Ti and its alloys. Pan et al.[16] used EIS to investigate the protective effect of the oxide layer and its relation to the presence of hydrogen peroxide (H_2O_2) in the media; their results confirmed the good stability of the oxide layer in the absence of peroxide and the accelerated corrosion process in the presence of peroxide. The authors also presented models of different stages of oxide layer formation with or without peroxide. With respect to the presence of alloying elements, Kolman et al.[17] conducted EIS to calculate the oxide layer thickness by considering a uniform layer on the surface; they detected a preferential formation of TiO_2 compared to other oxides. In addition, they presented an electrolyte resistance model using two parallel RC pairs, with the first pair as an oxide response (with oxide resistance and capacitance) and the second in the electrochemical domain (charge transfer resistance and double layer). In the same study, the authors previewed the deviation of the capacitor from ideal response and applied a constant phase element (CPE) to the model. The CPE led to intriguing EIS results[18-19]. More recently, a model has been applied to calculate oxide layer thickness under the assumption that the layer is uniformly distributed[20].

The ability to simultaneously develop micro- and nanotopographies has been demonstrated by the chemical etching of Ti and Ti6Al4V with an aqueous mixture of H_2SO_4 and H_2O (piranha solution). The resulting texture is advantageous for both short- and long-term osteogenic events in vitro, and the newly generated surface upregulates the expression of certain bone matrix proteins by culturing osteogenic cells[21-24]. The treatment time can affect the morphological and physicochemical characteristics of the nanoporous surface formed by this chemical oxidative patterning[25]; however, the effect of treatment temperature is still unknown. In addition, the effect of using a piranha solution on the wettability and corrosion resistance of the surface has not been reported yet. Therefore, the main objective of this study is to determine if treatment temperature can be used to tailor the physicochemical properties of Ti6Al4V alloy surface, including topography, chemistry, wettability and corrosion resistance.

2. Materials and Methods

2.1 Controlled chemical oxidation of Ti6Al4V samples

Ti6Al4V samples (chemical composition according to Grade 5 - ASTM B265[26]) with dimensions of 20 × 20 × 3 mm were mechanically polished to a mirror finished surface using SiC grinding papers (order of 180, 320, 400, 600, 1200, 1500 and 2000 grit), diamond paste, and a SiO_2 suspension (0,05 μm). The polished samples were then cleaned with acetone in an ultrasonic bath for 20 min and finally dried in air. The piranha solution used for etching was prepared by carefully adding pure (95%–98%, equivalent to 36 N) H_2SO_4 to an equal volume of 30% aqueous H_2O_2. The polished Ti6Al4V samples were immersed in the freshly prepared solutions and etched for 30 min at three different temperatures: 25 °C, 40 °C, and 60 °C; thus, three different conditions were obtained for the physicochemical analysis (in addition, the original untreated polished sample was considered as a control). During the etching, the samples were cooled on ice using a water bath (SolidSteel SSD 10L) to control the exotherm of mixing using a laboratory's thermometer, and then the cooling bath was removed to allow the temperature to rise, when necessary. The chemical reactions are reviewed elsewhere[27]. After the etching was completed, the samples were rinsed with distilled water, cleaned further using acetone in an ultrasonic bath for 20 min, and subsequently dried in air.

2.2 Surface characterization

The surfaces of the etched samples and the untreated controls were examined by using a scanning electron microscope (SEM) Tescan Mira 3; profilometer Veeco Wyko NT1100, diffractometer Rigaku Ultima IV (Cu K α radiation, λ= 0.15405 nm) at 40 kV, 30 mA and a grazing incident angle of ω = 0.5° in the 2θ range of 20°–85°. The surface wettability was evaluated by contact angle measurements. The contact angles of the samples were assessed by dropping 10 μL of distilled water on specimens and measured using an image-based goniometer (Theta Lite Biolin Scientific).

2.3 Corrosion tests

Corrosion resistance was evaluated by potentiodynamic polarization and EIS (performed by Metrohm Autolab PGSTAT302N potentiostat) in simulated body fluid (SBF); the chemical compositions of these fluids have been provided in Table 1. The potentiodynamic polarization curves were obtained in the potential window −0.8 to 1.5 V (vs. Ag/AgCl 3 M) in 1 mV steps and at a scan rate of 1 $mV.s^{-1}$. After potentiodynamic polarization, the samples were rinsed using pure water and dried with ethanol for further SEM analysis (Model INSPECT S50) to evaluate their morphological changes. Before each measurement, the samples were immersed in SBF for 1 h to stabilize. EIS experiments were performed at open-circuit potential with an amplitude of 10 mV and frequency range of 10^5–10^{-2} Hz. The measurements were evaluated by the Kramers–Kronig test and the equivalent circuit was fitted using software NOVA (Autolab). After immersing in SBF for 72 h, the samples were investigated by SEM.

Table 1. SBF chemical composition.

Reagents	Concentration
NaCl	8 g/l (146.7 mM)
$MgCl_2$	0.30 g/l (1.54 mM)
$CaCl_2.2H_2O$	0.368 g/l (2.5 mM)
$Na_2HPO_4.2H_2O$	0.178 g/l (1.0 mM)
$NaHCO_3$	0.352 g/l (4.2 mM)

3. Results and Discussion

3.1 Surface topography and morphology

Fig. 1 shows the changes in the surface topography of the Ti6Al4V samples with respect to etching temperature. The control sample (Fig. 1a) was flat and the treated samples showed peaks and valleys depending on variations in the etching temperature (Fig. 1b–d). A quantitative analysis of the surface root mean square (RMS) roughness was also performed based on the topographies of Fig. 1. The average and standard deviations are shown in Fig. 2. The quantitative analysis in Fig. 2 corroborated with the qualitative analysis of Fig. 1: the RMS roughness of Ti6Al4V increased exponentially with increasing temperature in the range studied. Fig. 3 shows the evolution of surface area after etching treatment. The peaks and valleys generated due to increased roughness provided a larger surface area than a completely flat surface. Increasing the surface area increased the area of contact between the metal and bone cells, improving the conditions for osseointegration[5-6]. From Fig. 3, it could be noted that increasing the etching temperature led to an exponential increase in the surface area. Even in the control sample, which was polished to a mirror finish and appeared to be flat, showed a small surface area increase of 0.005%, since this sample showed an RMS roughness of 19.5 ± 2.9 nm. The presence of apparently imperceptible peaks and valleys in the control sample could be better visualized when the scale of the optical profilometry images was adjusted for each image and not standardized for comparison, as shown in Fig. 1. Fig. 4 shows the optical profilometry images with the scale adjusted for each image; as shown, peaks and valleys were observed for all samples, even the control sample, and they became larger depending on the chemical attack.

To better understand how surface roughness varied on increasing the etching temperature, SEM analysis was performed. Fig. 5 shows the microstructure of the Ti6Al4V alloy under study. The microstructure exhibited a typical equiaxial structure containing α (hexagonal close-packed - hcp) and β (body centered cubic - bcc) phases. The β phase is characterized by low concentrations of aluminum and high concentrations of vanadium, since vanadium is the stabilizer in this phase. On the other hand, the α phase is characterized by low concentrations of vanadium and high concentrations of aluminum, since aluminum is the stabilizer in this phase[28]. Fig. 6 shows the difference in compositions of the phases,

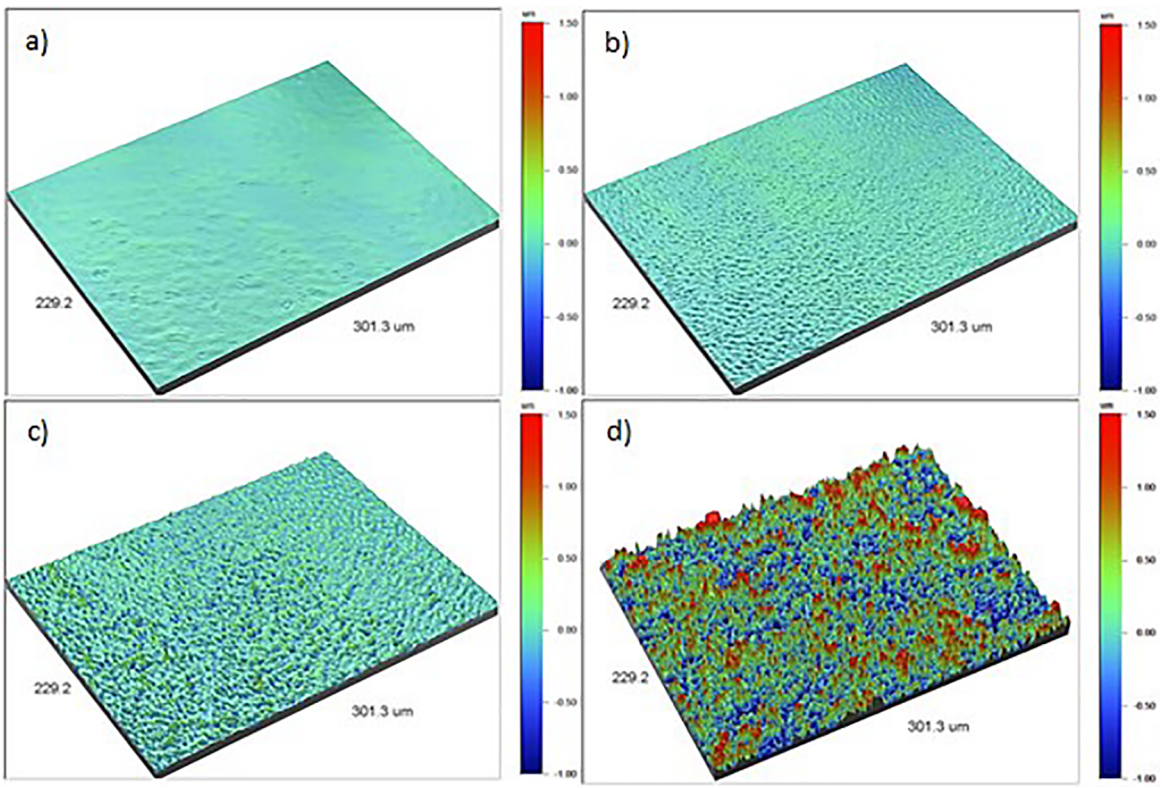

Figure 1. Profilometry topographies (area: 229.2 × 301.3 µm, scale: −1.0 to +1.5 µm) of polished Ti6Al4V samples. (a) untreated control and (b–d) surfaces exposed to piranha solution for 30 min at 25 °C, 40 °C, and 60 °C, respectively.

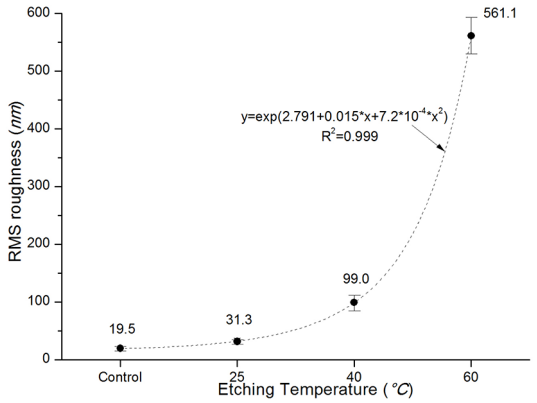

Figure 2. Ti6Al4V RMS roughness changes as a function of etching temperature.

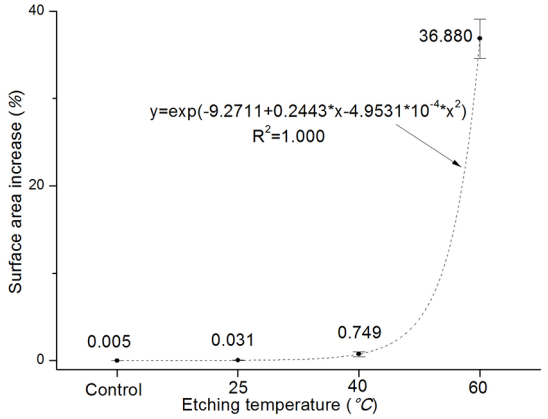

Figure 3. Ti6Al4V surface area changes as a function of etching temperature.

with a higher vanadium content observed in the β phase and a higher aluminum content observed in the α phase; this confirmed that the β phase presented interstitial grains surrounded by the α phase, as shown in Fig. 5.

SEM micrographs of the Ti6Al4V surface exposed to the piranha solution at various temperatures are shown in Fig. 7. As the etching temperature increased, the cavities corresponding to the β phase became more evident due to the difference in the rate at which the α and β phases were attacked. It is caused by the difference of electrochemical properties of the two phases: β-phase being more susceptible than the α-phase when exposed to piranha´s solution. High-resolution images in the inset of Fig. 7 provide more details about the surface. Before chemical etching (Fig. 7a), the surface showed an unaltered topography, showing only the grooves formed due to polishing. In the sample treated at 25 °C (Fig. 7b), the β phase was more strongly attacked than the α phase. The inset of Fig. 7b shows the formation of a nanotexture characterized by nanometric pits. When the sample was treated at 40 °C (Fig. 7c), the β-phase nanopits became even more evident, but the α phase was also attacked by the piranha solution; accordingly, the morphology of the α and β phases became increasingly similar at the nanometer scale, with the entire surface covered by nanopits and nanopeaks distributed throughout the matrix, leading to a sponge-like three-dimensional texture. In the sample etched at 60 °C (Fig. 7d), it was impossible to distinguish between the α and β phases. Further, the nanopits and nanopeaks could no longer be visualized, forming a uniform texture going from nano- to microtopography.

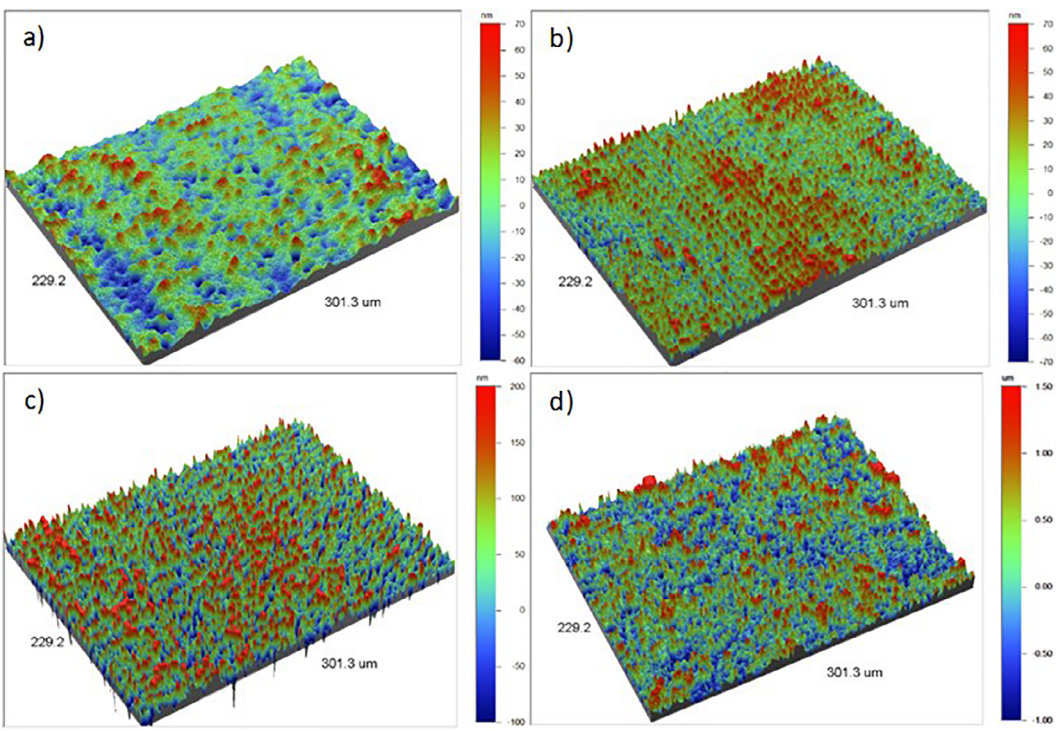

Figure 4. Profilometry topographies (area: 229.2 × 301.3 µm) of polished Ti6Al4V samples. (a) untreated control: scale −60 to 70 nm; (b) etched at 25 °C: scale −70 to 70 nm; (c) etched at 40 °C: scale −100 to 200 nm; and (d) etched at 60 °C: scale −1000 to 1500 nm.

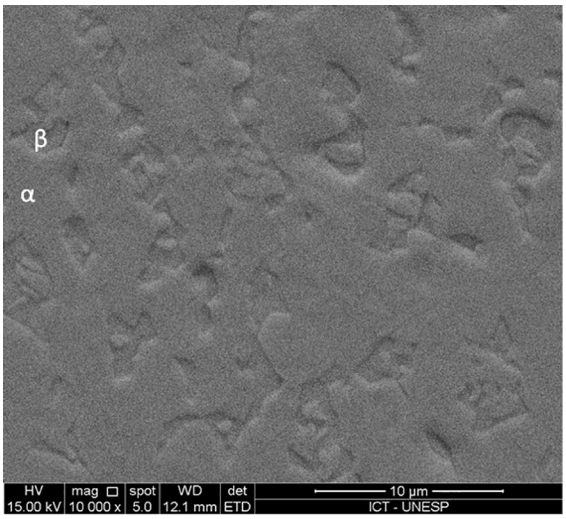

Figure 5. SEM image of control Ti6Al4V polished sample showing α and β phases.

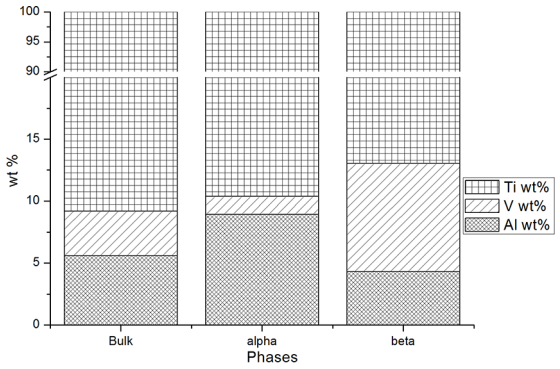

Figure 6. Weight percentages (wt%) of Al, V, and Ti in bulk alloy, α phase, and β phase, as measured by energy-dispersive X-ray spectroscopy of untreated Ti6Al4V sample.

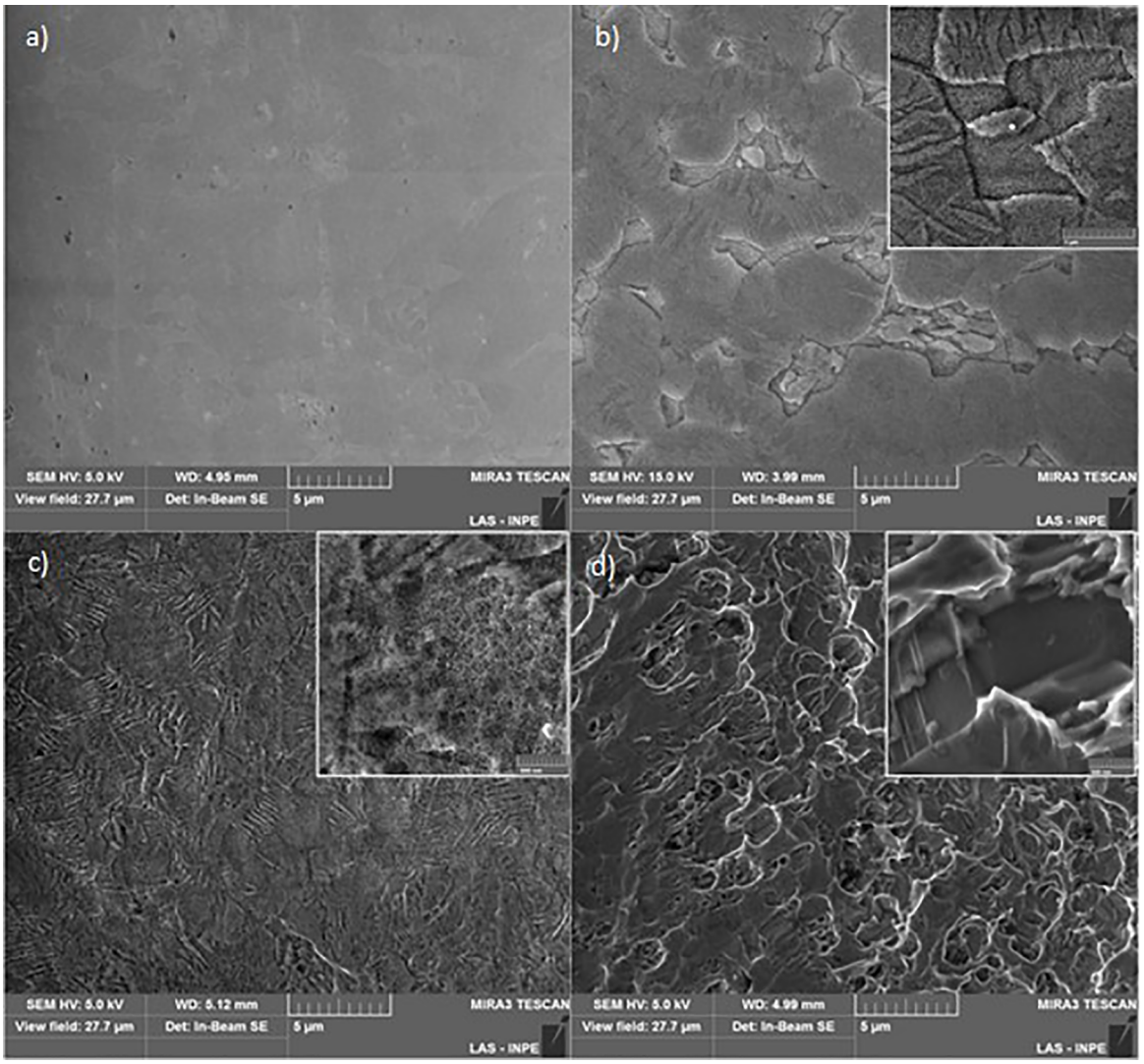

Figure 7. SEM images (10,000×) of polished Ti6Al4V samples. (a) untreated control and (b–d) samples etched by piranha solution for 30 min at 25 °C, 40 °C, and 60 °C, respectively. Insets show high-resolution images of nanotextures in (100,000×).

Variola et al.[25] reported a piranha solution attack under similar conditions but kept the temperature constant (22 ° C) and altered the etching time (15 min, 30 min, 1 h, 2 h, and 4 h). Their surface roughness and morphology results were similar to those reported in the present study, demonstrating that an increased treatment time led to increased roughness and altered surface texture. Therefore, increasing the etching temperature could provide the same result in a shorter time, which could be confirmed by the accelerated reaction kinetics. One factor accelerating the rate of reaction is the etching temperature. The rates of chemical reactions increase with increasing temperature. The increase in temperature increases the kinetic energy of molecules, and as molecules move faster, they collide more frequently and with higher energy, causing their reaction rates to increase. For a reaction to occur, the colliding molecules must have a total kinetic energy equal to or greater than a minimum value, called the activation energy E_a. At high temperatures, a larger fraction of molecules have a higher kinetic energy greater than E_a, which leads to a higher reaction rate. The increase in the reaction rate with increasing temperature is non-linear and is described by equation 1, proposed by Arrhenius[29]:

$$k = Ae^{-Ea/RT} \quad (1)$$

where k is the velocity constant, E_a is the activation energy, R is the gas constant, T is the absolute temperature, and A is the collision frequency factor. As the temperature T increases, the velocity constant k increases exponentially because the fraction of molecules possessing the required energy is larger. The exponential increase in the RMS roughness and surface area as a function of etching temperature can therefore be explained by the exponential increase in the reaction rate caused by the increase in temperature.

3.2 Surface chemistry (crystallinity)

XRD measurements (Fig. 8) of all samples showed similar features and no peak related to the anatase or rutile phase was recorded. It suggests that the amorphous TiO_2 was not changed to a crystalline structure or the layer is too thin that couldn't be detected. According to Cullity and Stock[30], the intensity of a diffracted beam is proportional to the volume of diffracting material and the diffracted beams will be very weak or entirely absent if the layer is too thin. This result is in agreement with those of previous studies on Ti6Al4V etched by a piranha solution, where crystalline TiO_2 was not observed[21-25].

3.3 Surface wettability

Table 2 shows the contact angles of the samples. According to Table 2, the mean contact angle values of the samples were very close to each other, but the standard deviation values greatly varied. The data were then statistically evaluated by analysis of variance (ANOVA) with 5% significance. The p value (0.99482) obtained is higher than the significance level

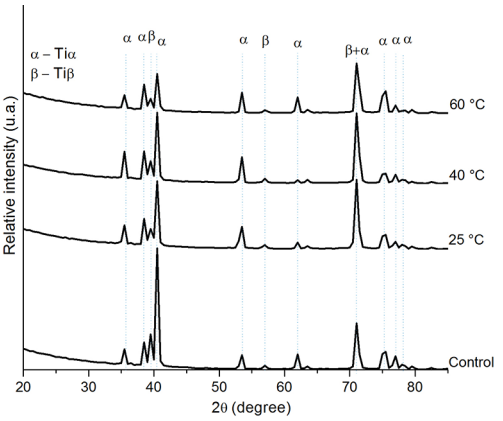

Figure 8. Grazing-angle XRD pattern of untreated control and surfaces exposed to piranha solution for 30 min at 25 °C, 40 °C, and 60 °C.

Table 2. Contact angles of Ti6Al4V control and surface-treated samples.

Treatment	Mean contact angle (°)	Standard deviation
Control	81.6	11.8
25 °C	82.7	24.8
40 °C	81.8	13.6
60 °C	79.9	6.2

chosen (0.05); therefore, there is no evidence of significant differences between the treatments. This suggests that the treatment does not alter the wettability of the surface, maintaining a moderately hydrophilic surface. The three most important factors that affect the wettability of a surface are its chemical composition, microstructural topography, and surface charge[27]. Although microstructural topography was changed in this work, the chemical composition and the surface charge was probably not changed enough to affect the wettability.

3.4 Corrosion resistance

Potentiodynamic polarization curves of the Ti6Al4V control and treated samples are shown in Fig. 9. The corrosion current densities were obtained from the polarization curves by extrapolation of the cathodic branch of the polarization curves to the corrosion potential, and the values are shown in Table 3. The corrosion current density values obtained from the potentiodynamic polarization curves decreased with increasing etching temperature, and this was assumed to be a direct consequence of oxide protective layer formation due to the oxidative treatment temperature[31].

After the potentiodynamic polarization, the samples were evaluated by SEM to verify any morphological modifications. Fig. 10 shows the SEM images of all samples. From these images, it was possible to comparatively check the reduction in degradation caused by potential scanning. It was also possible to verify the efficacy of increasing the chemical oxidation temperature to enhance the final corrosion resistance.

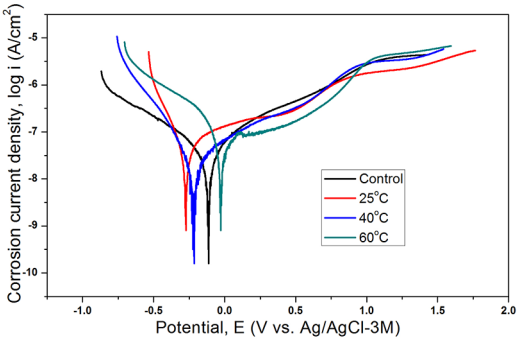

Figure 9. Potentiodynamic polarization curves in SBF of control sample and samples etched at different temperatures.

Table 3. Potentiodynamic polarization curve data of samples.

Sample	Corrosion potential (mV vs. Ag/AgCl - 3 M)	Current density ($nA.cm^{-2}$)
Control	−115.56	57.24
Treated at 20 °C	−273.73	55.24
Treated at 40 °C	−223.0	39.97
Treated at 60 °C	−33.11	34.47

The data obtained by EIS were validated by the Kramers–Kronig test[32]. The samples were adjusted according to the Kolman and Scully equivalent circuit[17] and the selected circuit is shown in Fig. 11. In this model, R_e corresponds to the electrolyte resistance, R_{ox} to the oxide resistance, R_{Ct} to the charge transfer resistance, Q_1 to the oxide capacitance, and Q_2 to the charge transfer capacitance.

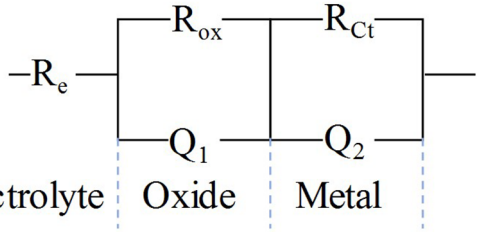

Figure 11. Equivalent circuit used to adjust experimental data.

Fig. 12 shows the Bode plot obtained from the EIS data (symbols) and equivalent circuit data fitted in a continuous line. The equivalent circuit model proposed by Pan et al.[16]

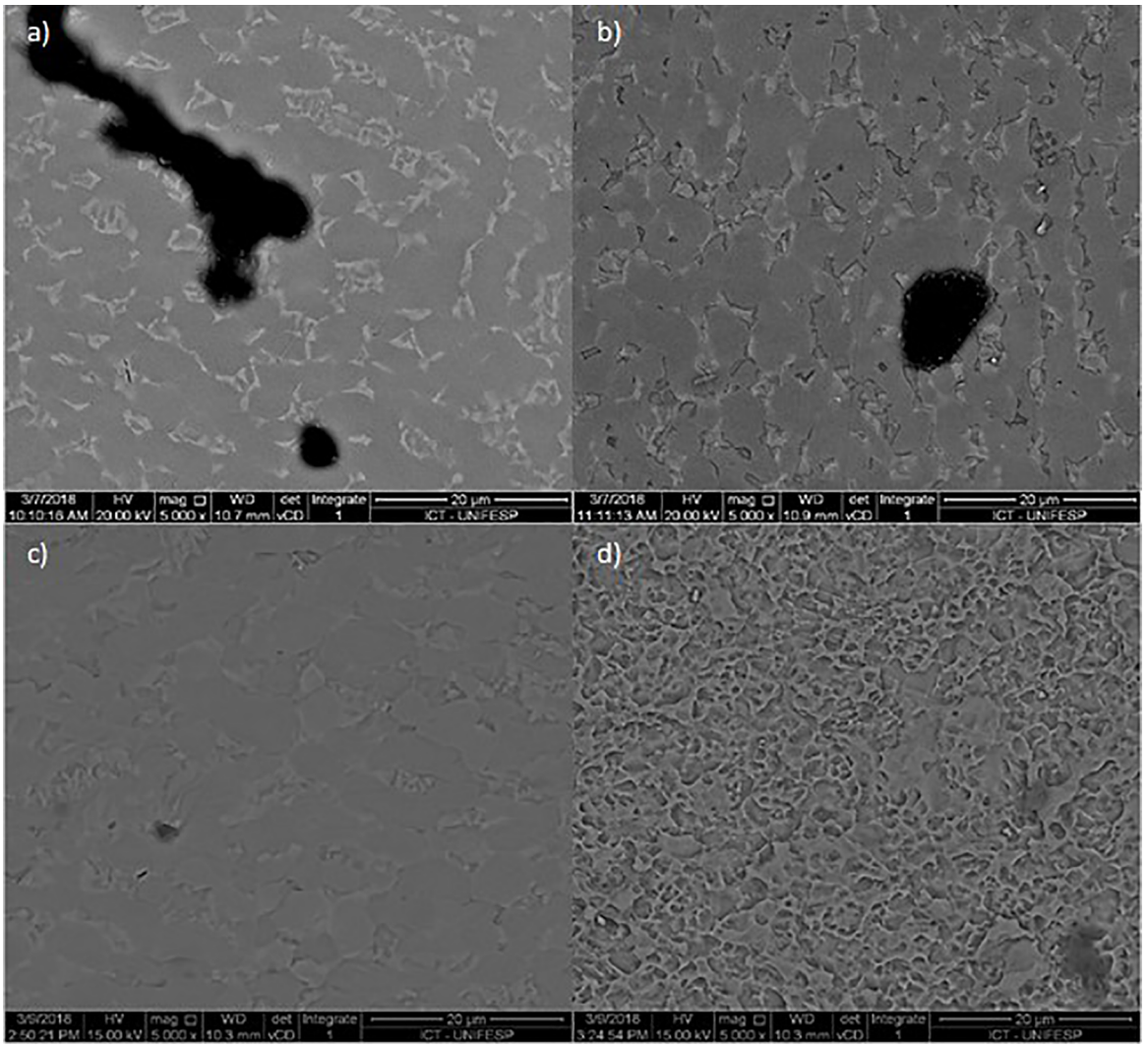

Figure 10. SEM images of Ti6Al4V samples after potentiodynamic polarization in SBF. (a) untreated control and (b–d) samples etched by piranha solution for 30 min at 25 °C, 40 °C, and 60 °C, respectively.

was selected for fitting the data. The convergence of the fitted data presented a chi-square close to 10^{-3}, allowing suitable adjustment for equivalent circuit data fitting. Table 4 presents the data obtained from the equivalent circuit. From Table 4, it could be observed that the sample treated at 25 °C showed an erratic response at low frequencies, suggesting oxidation or oxide layer formation during immersion in SBF. After 8 or 12 h of immersion, this behavior disappeared. This instability resulted in higher deviation of n_2 at the double-layer CPE (constant phase element). As a complex physicochemical system, a double layer at interface deviates from an ideal capacitor, and consequently the impedance formula doesn't describe correctly the electrochemical double layer capacitance[18-20]. We attributed the apparent higher R_{ct} of this sample to Ti complexation and incomplete TiO_2 gel formation in SBF. As expected from the potentiodynamic polarization curves, the EIS measurements also confirmed an increase in oxide resistance (R_{ox}) from 32 to 9232 Ω.cm^2 with increasing treatment temperature, and this result confirmed the great stability of the Ti6Al4V alloy. This increase may be related to the thickness of the oxide layer. Previous research provided the correlation between the thickness of the oxide layer and the effective capacitance of the oxide film[20]. The increase in the thickness of the oxide layer formed during etching of the Ti6Al4V alloy with a piranha solution at different times of exposure was estimated by Variola et al.[25] using ellipsometry. They observed that the oxide layer thickness increased from 5 nm in the untreated sample to 45 nm after 1 h exposure to the piranha solution at a temperature of 22 °C.

After 72 h of immersion, the samples were evaluated by SEM to detect morphological modifications. The results shown in Fig. 13 agree with the EIS results. From Fig. 13a and 13b, it could be observed that corrosion during SBF immersion was promoted in the untreated sample and in the sample treated at 25 °C. Clearly, both samples underwent corrosion, but the

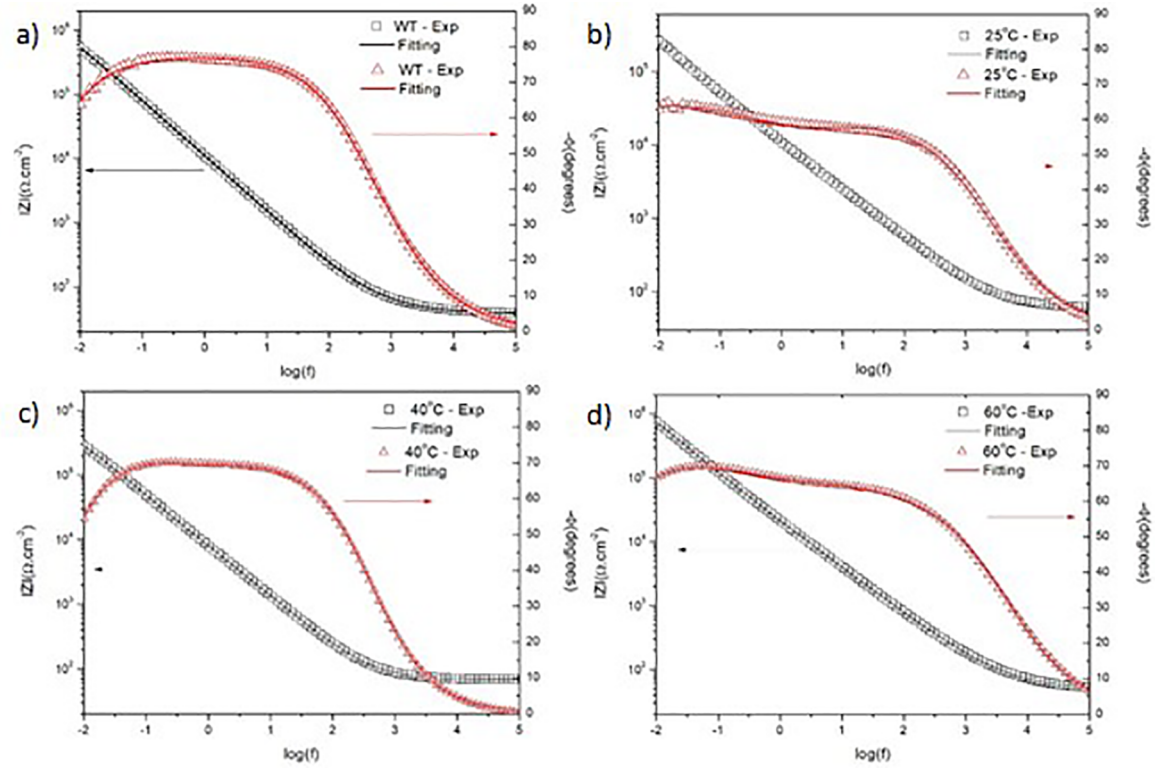

Figure 12. Bode plots of Ti6Al4V with experimental and fitted data. (a) untreated control and (b–d) samples etched by piranha solution for 30 min at 25 °C, 40 °C, and 60 °C, respectively.

Table 4. Electrical parameters of equivalent circuit obtained by fitting experimental results of EIS.

	R_e (Ω.cm^2)	R_{Ox} (Ω.cm^2)	Q1 (F.cm$^{-(n-1)}$)	n_1	R_{Ct} (MΩ.cm^2)	Q_2 (μF.cm$^{-(n-1)}$)	n_2	χ^2
Control	38.026 ± 0.228	32.68 ± 0.831	3.601E−4 ± 6.2E−7	0.56 ± 4.2E−4	2.41699 ± 1.99	18.54 ± 3.98	0.85 ± 0.035	8.4E−3
25 °C	57.334 ± 0.099	812.07 ± 26.46	1.479E−4 ± 2.153E−6	0.57 ± 1.9E−3	133.201 ± 256	33.30 ± 3.7E−2	0.76 ± 8.8E−4	1.8E−3
40 °C	67.583 ± 0.047	2584.19 ± 148.54	1.891E−4 ± 5.879E−6	0.68 ± 1.3E−3	0.808 ± 0.07	30.07 ± 8.1E−2	0.83 ± 1.4E−3	7.4E−4
60 °C	48.879 ± 0.132	9232.67 ± 1058.80	6.242E−5 ± 3.396E−6	0.59 ± 3.3E−3	7.18884 ± 0.51	12.10 ± 8.0E−2	0.81 ± 3.5E−3	4.0E−3

latter presented a lower density of local corrosion. Fig. 13c presents the surface treated at 40 °C; as shown, very small dots corresponding to the corrosion effect could be observed. Finally, the surface treated at 60 °C presented a notable morphology modification and some holes could be observed. These holes were caused by chemical oxidation and did not result due to corrosion, since the holes edges presented the same surface modification as chemical etching.

Therefore, potentiodynamic polarization and EIS evaluations agreed with each other and suggested that the corrosion resistance and oxide layer thickness of the Ti6Al4V samples increased with increasing treatment temperature.

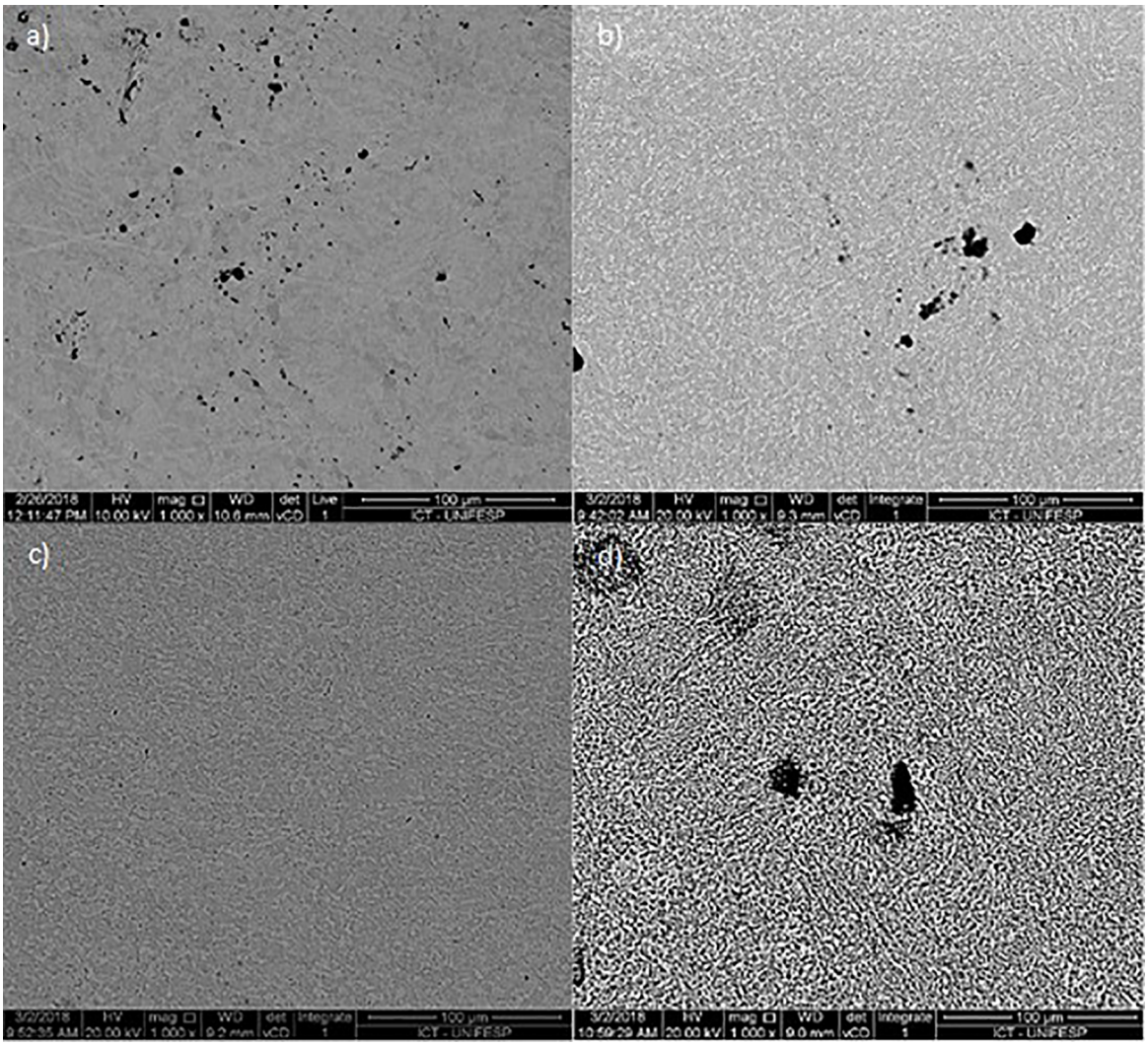

Figure 13. SEM images after 2 h immersion in SBF: (a) untreated control and (b–d) samples etched by piranha solution for 30 min at 25 °C, 40 °C, and 60 °C, respectively.

4. Conclusions

The study of the effect of etching temperature on the surface of the Ti6Al4V alloy used in biomedical applications allows us to conclude that it is possible to create a nano- and microtextured Ti6Al4V alloy surface by simple treatment with a H_2SO_4/H_2O_2 solution. The physicochemical properties of the surface, such as topography, roughness, surface area and corrosion resistance, can be tailored by modifying the temperature of the chemical attack. Moreover, wettability is not affected by the proposed treatment. The results show that it is possible to change the texture of the surface, with consequent increase in the roughness and surface area, while improving the corrosion resistance and oxide layer thickness. Considering that such properties are indirect indicators of potential success in the osseointegration of a dental implant, the surface treatment of Ti6Al4V alloy with a piranha solution at controlled etching temperatures is an attractive method of treatment.

5. Acknowledgements

This work was supported by CNPQ Universal [Grant number 403070/2016-3].

6. References

1. Pohler OEM. Unalloyed titanium for implants in bone surgery. *Injury*. 2000;31(Suppl 4):7-13.

2. Anderson JM. Biological responses to materials. *Annual Review of Materials Research*. 2001;31:81-110.

3. Duan K, Wang R. Surface modifications of bone implants through wet chemistry. *Journal of Materials Chemistry*. 2006;16(24):2309-2321.

4. Chang HI, Wang Y. Cell responses to surface and architecture of tissue engineering scaffolds. In: Eberli D, editor. *Regenerative medicine and tissue engineering - cells and biomaterials*. Rijeka: InTechOpen; 2011. p. 569-588.

5. Wennerberg A, Hallgren C, Johansson C, Danelli S. A histomorphometric evaluation of screw-shaped implants each prepared with two surface roughnesses. *Clinical Oral Implants Research*. 1998;9(1):11-19.

6. Brett PM, Harle J, Salih V, Mihoc R, Olsen I, Jones FH, et al. Roughness response genes in osteoblasts. *Bone*. 2004;35(1):124-133.

7. Bauer S, Schmuki P, Von Der Mark K, Park J. Engineering biocompatible implant surfaces part I: materials and surfaces. *Progress in Materials Science*. 2013;58(3):261-326.

8. Le Guéhennec L, Soueidan A, Layrolle P, Amouriq Y. Surface treatments of titanium dental implants for rapid osseointegration. *Dental Materials*. 2007;23(7):844-54.

9. Rupp F, Scheideler L, Olshanska N, Wild M, Wieland M, Geis-Gerstorfer J. Enhancing surface free energy and hydrophilicity through chemical modification of microstructured titanium implant surfaces. *Journal of Biomedical Materials Research Part: A*. 2006;76(2):323-34.

10. Paital S, Dahotre NB. Calcium phosphate coatings for bio-implant applications: materials, performance factors, and methodologies. *Materials Science and Engineering: R: Reports*. 2009;66(1):1-70.

11. Agrawal CM, Ong JL, Appleford MR, Mani G. *Introduction to biomaterials basic theory with engineering applications*. New York: Cambridge University Press; 2014.

12. Planell JA, Navarro M, Altankov G, Aparicio C, Engel E, Gil J. Materials surface effects on biological interactions. In: Shastri VP, Altankov G, Lendlein A, editors. *Advances in regenerative medicine: role of nanotechnology, and engineering principles*. Amsterdam: Springer Netherlands; 2010. p. 233-252.

13. Spector M. Biomaterial failure. *Orthopedic Clinics of North America*. 1992;23(2):211-217.

14. Manam NS, Harun WSW, Shri DNA, Ghani SAC, Kurniawan T, Ismail MH, et al. Study of corrosion in biocompatible metals for implants: A review. *Journal of Alloys and Compounds*. 2017;701:698-715.

15. Healy KE, Ducheyne P. Oxidation kinetics of titanium thin films in model physiologic environments. *Journal of Colloid and Interface Science*. 1992;150(2):404-417.

16. Pan J, Thierry D, Leygraf C. Electrochemical impedance spectroscopy study of the passive oxide film on titanium for implant application. *Electrochimica Acta*. 1996;41(7-8):1143-1153.

17. Kolman DG, Scully JR. Electrochemistry and passivity of a Ti-15Mo-3Nb-3Al beta-titanium alloy in ambient temperature aqueous chloride solutions. *Journal of The Electrochemical Society*. 1993;140(10):2771-2779.

18. Hsu CH, Mansfeld F. Concerning the conversion of the constant phase element parameter Y0 into a capacitance. *Corrosion*. 2001;57(9):747-748.

19. Brug GJ, Van Den Eeden ALG, Sluyters-Rehbach M, Sluyters JH. The analysis of electrode impedances complicated by the presence of a constant phase element. *Journal of Electroanalytical Chemistry and Interfacial Electrochemistry*. 1984;176(1-2):275-295.

20. Hirschorn B, Orazem ME, Tribollet B, Vivier V, Frateur I, Musiani M. Constant-phase-element behavior caused by resistivity distributions in films I. Theory. *Journal of The Electrochemical Society*. 2010;157(12):C452-C457.

21. Nanci A, Wuest JD, Peru L, Brunet P, Sharma V, Zalzal S, et al. Chemical modification of titanium surfaces for covalent attachment of biological molecules. *Journal of Biomedical Materials Research*. 1998;40(2):324-35.

22. Yi JH, Bernard C, Variola F, Zalzal SF, Wuest JD, Rosei F. Characterization of a bioactive nanotextured surface created by controlled chemical oxidation of titanium. *Surface Science*. 2006;600(19):4613-21.

23. Oliveira PT, Nanci A. Nanotexturing of titanium-based surfaces upregulates expression of bone sialoprotein and osteopontin by cultured osteogenic cells. *Biomaterials*. 2004;25(3):403-13.

24. Oliveira PT, Zalzal SF, Beloti MM, Rosa AL, Nanci A. Enhancement of in vitro osteogenesis on titanium by chemically produced nanotopography. *Journal of Biomedical Materials Research: A*. 2007;80(3):554-64.

25. Variola F, Yi JH, Richert L, Wuest JD, Rosei F, Nanci A. Tailoring the surface properties of Ti6Al4V by controlled chemical oxidation. *Biomaterials*. 2008;29(10):1285-98.

26. ASTM - American Society for Testing and Materials. *B265-15 – Standard Specification for Titanium and Titanium Alloy Strip, Sheet, and Plate*. West Conshohocken, USA: ASTM International; 2013.

27. Wen C. *Surface Coating and Modification of Metallic Biomaterials*. Cambridge: Woodhead Publishing; 2015.

28. Balazic M, Kopac J, Jackson MJ, Ahmed W. Review: titanium and titanium alloy applications in medicine. *International Journal of Nano and Biomaterials*. 2007;1(1):3-34.

29. Brown TE, LeMay HE, Bursten BE, Murphy C, Woodward P, Stoltzfus ME. *Chemistry: The Central Science*. 14th ed. Harlow: Prentice Hall; 2017.

30. Cullity BD, Stock SR. *Elements of X-ray diffraction*. 3rd ed. Harlow: Pearson; 2001.

31. Assis SL, Wolynec S, Costa I. Corrosion characterization of titanium alloys by electrochemical techniques. *Electrochimica Acta*. 2006;51(8-9):1815-1819.

32. Boukamp BA. A Linear Kronig-Kramers Transform Test for Immittance Data Validation. *Journal of The Electrochemical Society*. 1995;142(6):1885-1894.